Ultrafast changes in optical properties of SiO 2 excited by femtosecond laser at the damage threshold and above

C. Fourment, B. Chimier, F. Deneuville, D. Descamps, F. Dorchies, G. Duchateau, C. Nadeau, S. Petit

Ultrafast changes in optical properties of SiO_2 excited by femtosecond laser at the damage threshold and above

C. Fourment,[1,2,*] B. Chimier,[1] F. Deneuville,[1] D. Descamps,[1] F. Dorchies,[1]
G. Duchateau,[1] M.-C. Nadeau,[1] and S. Petit[1]
[1]*Université de Bordeaux-CNRS-CEA, Centre Lasers Intenses et Applications (CELIA), Talence, F-33405, France*
[2]*CEA-DAM-CESTA, Le Barp, F-33114, France*

(Received 10 February 2018; revised manuscript received 28 June 2018; published 3 October 2018)

A time- and polarization-resolved pump-probe reflective interferometry measurement of fused silica excited by a femtosecond laser pulse above the damage threshold is presented. We compare the evolution of both the amplitude and the phase of the reflectivity with a rate equation coupled with a Drude model, widely used to interpret pump-probe experiments where a laser probe interacts with an excited semiconductor or dielectric. Despite the success reported in literature of such a model to reproduce experiments on a wide band-gap dielectric below the damage threshold, we show that it is not valid in the regime of interaction explored in this paper. The dielectric function at the laser wavelength is directly retrieved from our measurements, and several hypotheses are proposed to account for the observations.

DOI: 10.1103/PhysRevB.98.155110

I. INTRODUCTION

The interaction between an ultrashort (100-fs typical) and intense laser pulse (USLP) with a dielectric material has been a topic of great and continuous interest for decades [1–21], both for the fundamental physics challenge and for the applications especially regarding micromachining and damage threshold improvement of optical components in the femtosecond regime. The interaction is driven by the primary process, which is the free-carrier generation, and the relaxation of energy. Theoretical modeling of the electron population is extremely hard due to the number and complexity of the potentially implied processes: (i) electron excitation by the optical field from the valence band (VB) to the conduction band (CB) of the dielectric which leads to a nonthermal conduction electron population, (ii) collisional processes between the electrons and with the other species (including photons and phonons) leading to thermalization and heating, and (iii) photoinduced modification of the electronic band structure in the material. The first two points have been widely addressed at different degrees of refinement (see, e.g., papers [6,17,22] and references therein) but still neglecting the photoinduced modification (iii). Conversely, the description of the electronic structure in excited dielectrics has been performed in few specific cases with crude approximations regarding the excitation and thermalization of the electrons [8,23]. The influence of such a mechanism has been found to be of prime importance during the USLP excitation of semiconductors at a level close to the permanent damage threshold [24], but taking it into account is not mandatory to reproduce the refractive index evolution in moderately excited wide band-gap dielectrics [4]. Recently, a copious band-gap shrinkage has been evoked to account for a potential laser amplification just after the excitation of sapphire and fused silica by USLP [21]. However no convincing direct proof of such a mechanism has been given. In the absence of a unified description and experimental data, the role of the process (iii) in the interaction of the USLP with a dielectric close to the damage threshold is still an open question. In this context, the simplified description where the excitation re-distributes the electrons in the fixed scaffold of energy levels and the excited electrons follow a Drude-like behavior is still widely used. The aim of our paper is to test this simple description in a condition of strong excitation.

Addressing experimentally such a question is challenging because of the required time resolution, typically shorter than 100 fs. Indeed, the lifetime of the excited electrons in the conduction band in SiO_2 is about 150 fs [2], and bond breaking is likely to occur on the picosecond timescale or shorter [11]. Probing an excited sample with a femtosecond laser is a very convenient way to achieve the time resolution needed since the probe can be very short and is naturally synchronized with the beam used to excite the sample. Such a pump-probe interferometry technique has been used by Martin *et al.* to investigate the dynamics of free carriers in wide band-gap dielectrics at a moderate level of excitation [4]. The authors measured the phase shift of the probe beam as it passed through the excited sample (transmission interferometry), but they were not able to study a regime of interaction close to the damage threshold due to the probe transmission configuration since the very high absorption of the probe light limited the accuracy of the experiment [20]. This is not the case with the experiment reported here as we performed pump-probe interferometry in a reflection geometry. Moreover, we measured both the phase and the amplitude of the probe beam in both directions of polarization S and P. This allowed us to measure the time evolution of the dielectric function of fused silica at a level of excitation above the permanent damage threshold and up to the ablation regime. At this irradiation level, our measurements show that the simplified description recalled

*claude.fourment@cea.fr

before lacks a major ingredient to describe the interaction of USLP with fused silica, which may be the modification of the electronic band structure and/or a non-Drude-like behavior of the excited electrons.

II. EXPERIMENT

A. Experimental setup

We realized a pump-probe frequency domain interferometry (FDI) [25] experiment (Fig. 1) with the use of the Aurore laser facility (800 nm, 30 fs, and 6 mJ at a 1-kHz repetition rate). Our diagnostic [26,27] allows us to measure the variations of the spectral components (amplitude and phase) of a probe pulse relative to a reference one with a 5-μm one-dimensional (1D) transverse spatial and 45-fs temporal resolutions. At first, the Aurore laser beam was split into two arms to generate synchronized pump and probe beams. Each pump and probe beam has a dedicated compressor with an output pulse duration of 30 fs (FWHM) measured with a 2ω autocorrelator. The pump beam was focused with a $f/40$ aperture by a fused-silica lens on the target within a 48 ± 1-μm FWHM spot size. The incident angle of the pump beam with respect to the target normal was set to 5° with S polarization. The pump beam energy was varied with a half-wave plate placed before a polarizer. We carefully characterized the focal pump spot by imaging it on a CCD camera with a microscope objective. This gives us a direct correspondence between the spatial position in the spot and the intensity. Thanks to a rotating target holder, the sample was refreshed for kilohertz laser operation so that each pump pulse interacted with a fresh and clean target surface. The probe beam was used to set up the FDI system. Both the reference and the measuring pulses were obtained by inserting a Michelson interferometer with a 24-ps time delay between them. These pulses were then focused by a spherical mirror used at quasinormal incidence (≈2°) to a 250-μm focal spot diameter on the target. The probe beam was set at 45° incidence with respect to the target normal (50° off the pump beam direction) with a linear polarization containing both S and P components. The first pulse (the reference pulse) is reflected on the target before the excitation by the pump beam, whereas the second one (the measuring pulse) is reflected after at a time set by a delay line in the pump beam path. The reflected probe beam was collected by a $f/5$ aperture aplanatic lens which imaged the target surface on the entrance of a 1-m focal-length Fastie-Ebert imaging spectrometer where both probe pulses spectrally interfered. A Wollaston cube was placed before the spectrometer CCD to spatially separate the S and P components. Accumulating 1000 shots for each pump-probe delay and using a cooled 16-bit CCD allowed us to use low-energy probe pulses (5-μJ typical) and to get interferograms with high signal-to-noise ratios. For each interferogram, a Fourier-transform-based algorithm is used to deduce the phase shift and the reflectivity variation (in this paper, the reflectivity is the field reflectivity, i.e., the square root of the usual energy reflectivity) at the corresponding delay with respect to the unheated sample. In addition, our Fourier-transform treatment of the spectral interferences allows for filtering out any noncoherent light (such as plasma emission) as well as the light of the pump beam which could be scattered (except when the pump and probe beams overlap temporally, which will be discussed later). Finally, the phase shift and the reflectivity variation are measured with 10 mrad and 1% accuracy, respectively.

The target was a 10-mm-thick optical quality fused-silica window. Owing to this thickness and the 45° angle of observation, no light reflected from the back side of the window reached the FDI spectrometer. We measured the phase shift and the reflectivity variation of the probe beam up to 5 ps after the excitation for three intensities of the pump beam: 160, 75, and 57 $\times$ 10^{12} W cm^{-2}. These values correspond to the maximum pump intensity, i.e., at the center of the 48-μm FWHM focal spot, and we estimate the uncertainty on the absolute value of the intensities to be ±10%. Thanks to the 1D transverse spatial resolution of our spectrometer, we are able to retrieve the phase shift and the reflectivity variation for any intensity in the range of 0–160 $\times$ 10^{12} W cm^{-2} by selecting the appropriate spatial area of the interferogram. Postmortem analyses were performed with a Nomarsky microscope and optical profilometer. After 160 $\times$ 10^{12} W cm^{-2}, the profilometer shows a 52 ± 2-μm diameter and 200 ± 10-nm

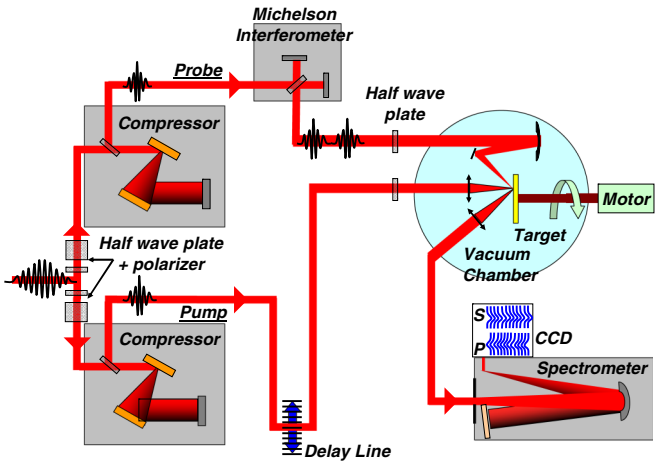

FIG. 1. FDI experiment setup.

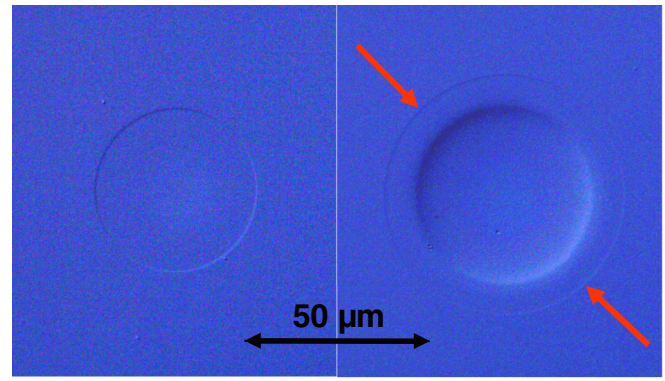

FIG. 2. Nomarsky microscope images of the SiO_2 sample after irradiation by one laser pulse of the center intensity of 75 $\times$ 10^{12} W cm^{-2} (left) and 160 $\times$ 10^{12} W cm^{-2} (right). The pronounced feature in the right image is a 200 ± 10-nm depth hole, whereas the light feature highlighted by the red arrows is a damage without ablation (no measurable depth).

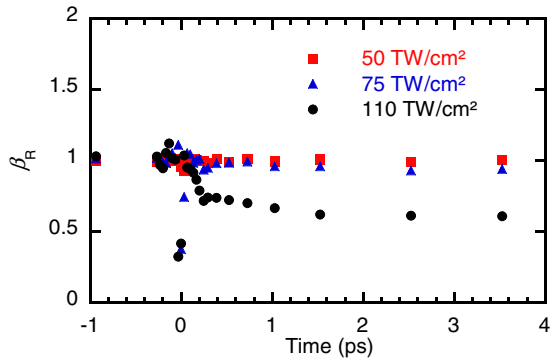

FIG. 3. Time evolution of $\beta_R = R_P/R_S^2$ for three intensities below (50), around (75), and above (110 TW cm^{-2}) the ablation threshold on the SiO_2 sample. The error bars are approximately the size of the symbols.

depth holes. The Nomarsky microscopy shows the same ablated zone, surrounded by a larger one with a 65 ± 1-μm diameter (see Fig. 2, right). This larger zone corresponds to a damaged zone, i.e., where there is a permanent modification of the optical index but without ablation. This damaged zone is also visible with a smaller diameter when 75×10^{12}-W cm^{-2} (Fig. 2, left) and 57×10^{12}-W cm^{-2} (not shown) intensities are used. Comparing the diameter of the zones with the profile of the pump beam allows us to determine the damage and ablation thresholds to be 45×10^{12} and 75×10^{12} W cm^{-2}, respectively. These thresholds are in reasonable agreement with published data [5,10,16]. Note that the probe pulse intensity on target was estimated to be 2×10^{11} W cm^{-2}, more than two orders of magnitude lower than the damage threshold of our SiO_2 sample.

B. Sample surface sharpness

Our FDI diagnostic allows us to follow the femtosecond-scale dynamics of the optical reflectivity variation and phase shift after irradiation. We have shown in previous works [26,28] that the comparison of the S and P probe components permits characterizing the interface between the material and the vacuum. The ratio $\beta_R = R_P/R_S^2$ is a relevant quantity for the sharpness of the interface: $\beta_R \approx 1$ indicates a sharp (Heaviside) vacuum-target interface, whereas a finite gradient length gives $\beta_R < 1$. In the case of a sharp interface, the phase-shift difference $\beta_\phi = 2\phi_S - \phi_P$ is equal to the Doppler phase shift due to the motion of the interface with respect to its initial position. Thus in this case, we can correct our data from the Doppler effect and obtain the phase shifts due only to the reflection on the surface,

$$\phi_S^{\text{opt}} = \phi_S - \beta_\phi,$$
$$\phi_P^{\text{opt}} = \phi_P - \beta_\phi, \quad (1)$$

where the superscript *opt* stands for the phase shifts due only to the modification of the optical properties of the sample. The time evolution of β_R for three intensities below, around, and above the ablation threshold are depicted in Fig. 3. The very sharp feature around $t = 0$ (at which the pump pulse excites the sample) is not to be considered here and will be discussed below. This figure shows that above the ablation threshold, the target material undergoes a plasma-type expansion with a finite gradient length immediately after the excitation ($\beta_R < 1$), which could alter the reflectivity and the transmission of the interface. On the contrary, below this threshold, the SiO_2 vacuum interface stays sharp ($\beta_R \approx 1$). Then the reflectivity and phase shift depend only on the optical properties of the sample, which can be extracted from the FDI data by inverting the Fresnel equations (see Appendix A). For this reason, in the following sections we focus on this last situation, i.e., for excitation intensity below the ablation threshold.

C. Coherent artifact

The time evolution of the probe reflectivity and phase shift relative to the unexcited sample for a 50-TW cm^{-2} pump pulse is depicted in Fig. 4. The dispersion of the data at the negative delays gives an idea of the error bar of our diagnostic. For the delays greater than ≈30 fs, the measures verify very well the relations $R_P = R_S^2$ and $\phi_P = 2\phi_S$ as expected for a Fresnel reflection at 45° incidence. However, during roughly 60 fs (which corresponds to the duration of the temporal overlap between the pump and the probe pulses) around $t = 0$, these relations are not fulfilled: The reflectivity and phase shift of the probe S component show strong variations, whereas the P component stays apparently unaffected (this situation corresponds to the large spikes of β_R and β_ϕ in Fig. 4). The maximum of the S reflectivity (close to $t = 0$) scales as I_p^α with I_p as the pump pulse intensity and $\alpha \approx 7 \pm 1$. This scaling excludes the pump-pulse-induced Kerr effect (which

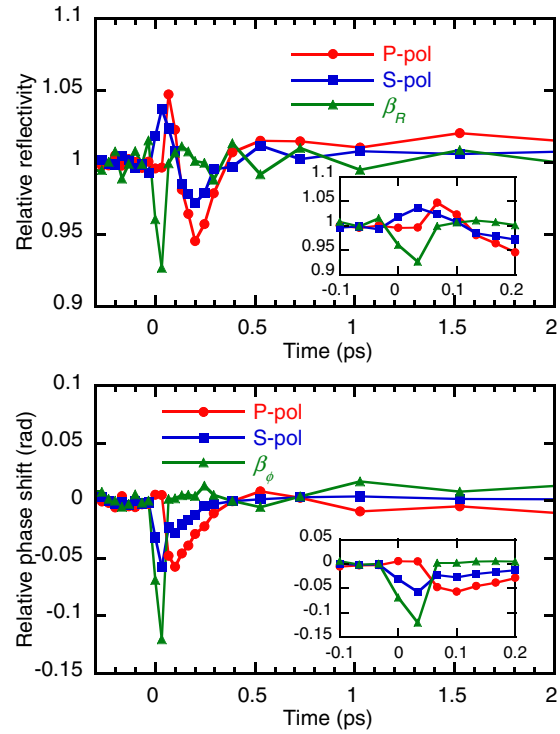

FIG. 4. Time evolution of the reflectivity (top) and phase shift (bottom), relative to an unexcited SiO_2 sample when a 50-TW cm^{-2} pump pulse excitation is used. The insets show a zooming for the very short delays.

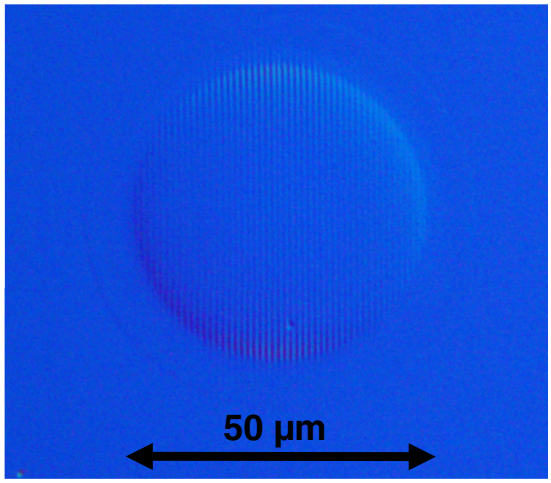

FIG. 5. Nomarsky microscope image of the SiO_2 sample when pump and probe pulses temporally overlap. The center intensity of the pump pulse is 160 TW cm^{-2}.

scales as I_p) as a possible cause of our observation. In order to understand the origin of this feature, we performed two tests : First, we rotate the direction of polarization of the pump by using a half-wave plate from the *S* to the *P* polarization. In this configuration, the sharp feature was observed only on the *P* component of the probe beam. Second, we frequency doubled the probe beam by using a 200-μm-thick β barium borate crystal. In this case, no sharp feature was observed in *S* or *P* polarization. This indicates that a coherent mechanism is at play. Such "coherent artifacts" are commonly observed in pump-probe experiments [29–31] in various configurations. In our experiment, it is due to the diffraction by an optical index grating induced by the spatial interference of the pump and probe beams in the special case of a highly nonlinear absorption regime. A rigorous description of such a mechanism is beyond the scope of this paper, but an intuitive description based on a local response of the surface allows for retrieving the main features of our observation (see Appendix B). Moreover, the observation depicted in Fig. 5 clearly shows a grating structure imprinted in the damages when pump and probe beams overlap temporally and only at this time. The measured spatial fringe distance is 1.00 ± 0.01 μm, in perfect agreement with Eq. (B1), which gives 1.007 μm. We conclude that the signals contain a spurious part due to the coherent artifact when pump and probe pulses overlap in time. On the contrary, as soon as the pump and probe pulses are time delayed enough (i.e., more than ≈50 fs), there is no coherent artifact, and the linear response of the pump-excited material is obtained from the collected probe light.

III. FIXED STRUCTURE WITH A DRUDE-LIKE MODEL

The literature reports that the optical response of various excited wide band-gap dielectrics has been successfully modeled at moderate pump irradiance, well below the damage threshold [2,4]. In this model, the electron band structure is assumed not to change during and after the pump irradiation. The effect of the excitation is to promote some electrons from the VB to the CB of the dielectric where they give to the optical properties a plasma-type component described by the Drude model. In addition, the electrons in the conduction band could decay and become trapped somewhere in the gap. The aim of our paper is to test the validity of this model in a regime of high excitation above the damage threshold. To maintain continuity with the low excitation conditions, we will choose for the input parameters the same values as detailed in the following. The electronic populations are described by their density N_{CB} in the CB and N_{tr} in the trapped states, and the dielectric function writes

$$\epsilon_{fs} = 1 + \frac{e^2}{m\epsilon_0}\frac{(N_0 - N_{\mathrm{CB}} - N_{\mathrm{tr}})f_{\mathrm{gap}}}{\omega_{\mathrm{gap}}^2 - \omega^2 + i\omega\nu_{\mathrm{gap}}} + \frac{e^2}{m^*\epsilon_0}\frac{N_{\mathrm{CB}}f_{\mathrm{CB}}}{-\omega^2 + i\omega\nu_{\mathrm{CB}}} + \frac{e^2}{m\epsilon_0}\frac{N_{\mathrm{tr}}f_{\mathrm{tr}}}{\omega_{\mathrm{tr}}^2 - \omega^2 + i\omega\nu_{\mathrm{tr}}}, \quad (2)$$

where the subscript *fs* stands for the frozen structure assumption. Note that throughout this paper, we adopt the convention $e^{+i\omega t}$ to describe the temporal dependence of the fields. In Eq. (2), e is the elementary charge, m is the electron mass, ϵ_0 is the vacuum permittivity, and ω is the probe pulsation. f_{gap}, ω_{gap}, and ν_{gap} are effective parameters representing the set of transition between the VB and the CB, standing for the oscillator strength, the energy difference between the VB and the CB, and the width of the transition, respectively. The corresponding term in Eq. (2) is called the Lorentz term. N_0 is the initial electron density in the valence band, $N_0 = 1.76 \times 10^{23}$ cm^{-3} corresponds to eight valence electrons in the fused silica at a density of 2.2 g/cm^3 (some authors consider one effective electron in the VB per SiO_2 molecule, giving 2.2×10^{22} cm^{-3}, but the actual value is not critical since it is much greater than N_{CB} and multiplied by the adjustable parameter f_{gap}). We fix $\omega_{\mathrm{gap}} = 9$ eV and $\nu_{\mathrm{gap}} = 0$ Hz for the fused silica at an 800-nm wavelength. $f_{\mathrm{gap}} = 0.36$ is set to obtain the value of 1.45 for the optical index of unexcited fused silica [32]. In the same way, f_{tr}, ω_{tr}, and ν_{tr} represent the transition undergone by the trapped states. These states are identified as self-trapped excitons (STEs), located about 6 eV under the CB in amorphous silica [15]. $\nu_{\mathrm{tr}} = 1.5$ eV stands for the width of the trapped states, and f_{tr} is on the order of unity [4]. In the Drude term, m^* is the electron effective mass in the CB (fixed to half the free-electron mass [4]), $f_{\mathrm{CB}} = 1$ [4] is the oscillator strength for the transitions occurring in the CB, and ν_{CB} is the momentum damping frequency for the electron in the CB. The assumptions of the model imply that most of the parameters in Eq. (2) are constant. Only N_{CB}, N_{tr}, and ν_{CB} evolve due to the pump laser excitation and the subsequent relaxation. The evolutions of N_{CB} and N_{tr} are described by a set of coupled rate equations,

$$\frac{dN_{\mathrm{CB}}}{dt} = \left(\frac{dN_{\mathrm{CB}}}{dt}\right)_{LI} - \frac{N_{\mathrm{CB}}}{\tau}, \quad (3)$$

$$\frac{dN_{\mathrm{tr}}}{dt} = \frac{N_{\mathrm{CB}}}{\tau}, \quad (4)$$

where the first term on the right-hand side of Eq. (3) is the laser ionization (LI) from the VB to the CB, and the second one describes the electron trapping with a time constant of $\tau \approx 150$ fs [2]. The impact ionization, which may lead to an electron avalanche, is not introduced here since it is negligible

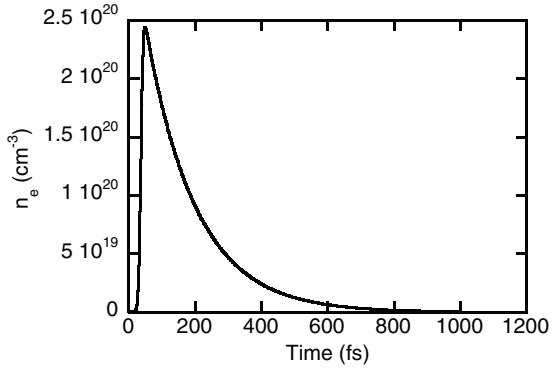

FIG. 6. Calculated electron density in the CB as a function of time when a SiO_2 sample is irradiated by a 30-fs pump pulse at an intensity of 50 TW cm^{-2}.

for the duration and intensity of the laser pulses that we use. Calculations based on the Boltzmann kinetic equations [6] as well as multiple rate equations [12] have shown that it is the case for laser durations shorter than roughly 100 fs up to 100 TW cm^{-2}. This is also evidenced by the comparison of calculated and measured transmissivity and reflectivity of fused silica irradiated by 800-nm, 90-fs laser pulses [9]. In the work cited previously [2,4], ν_{CB} was considered as a constant parameter, and the laser ionization term was explicitly described by a multiphoton ionization (MPI). Here we improve the model on these two aspects. First, since the time resolution of our pump-probe experiment is potentially shorter than the electron thermalization in the CB, we describe the CB electrons by their energy distribution function driven by a Boltzmann kinetic equation including the significant collisional and noncollisional processes [33]. We evaluate ν_{CB} in Eq. (2) as the average electron momentum damping frequency. However, we stress that this average damping frequency varies only within ±25% for the time and intensity ranges considered in this paper, and the overall results are not fundamentally different if we consider a constant frequency ν_{CB} on the order of 1 fs^{-1}. Second, we calculate the laser ionization by Keldysh theory [1] since we cannot consider pure MPI for the range of intensity addressed in this paper [16]. Figure 6 shows the electron density in the CB as a function of time calculated for a 30-fs pump pulse at an intensity of 50 TW cm^{-2} (in this figure, the maximum of the laser pulse is at 35 fs). At the end of the pump irradiation (at ≈50 fs) the electron density reaches its maximum value then decreases due to the electron trapping [see Eq. (4)]. At 1 ps, almost all the electrons in the CB have decayed in the trapped states. The maximum electron density in the CB is only a fraction of the ideal plasma critical density ($n_{ipc} = \epsilon_0 m\omega^2/e^2 = 1.75 \times 10^{21}$ cm^{-3}) for the range of intensity addressed.

For numerical simplification, the pump laser intensity I_p in the bulk of the target is assumed to be homogeneous. It takes into account the transmission at the vacuum-target interface which is calculated consistently by the Fresnel relations using the dielectric function of Eq. (2). To test the validity of the simplified homogeneous description, we made some comparisons with a more realistic calculation containing a self-consistent description of the laser absorption in the bulk [by both the laser ionization and the linear absorption, the last being deduced from the dielectric function of Eq. (2)]. Then the dielectric function is not homogeneous, and the reflectivity is computed by solving the Helmoltz wave equation in a transfer-matrix formalism [34]. We found less than a 20% difference in the final results, validating the homogeneous description. Finally, a Kerr term $n_2 I_p$ ($n_2 \approx 3 \times 10^{-16}$ cm^2/W in fused silica [35]) is added to the optical index before the computation of the reflectivity and phase shift from the Fresnel relations. In order to compare directly the simulation with the experimental data, the reflectivity and phase shift are computed relative to the values obtained for an unexcited sample where the optical index is set to 1.45 and convolve the results with a 45-fs FWHM Gaussian representative of the temporal resolution of the FDI diagnostic. Table I summarizes the parameters used in the model.

TABLE I. Set of parameters used in the simulation.

Initial valence electron density (cm^{-3})	N_0	1.76×10^{23}
Gap energy (eV)	ω_{gap}	9
Oscillator strength VB-CB	f_{gap}	0.36
Electron effective mass in the CB (kg)	m^*	4.55×10^{-31}
Oscillator strength for the CB	f_{CB}	1
Electron trapping time (fs)	τ	150
Trap level energy (eV)	ω_{tr}	6
Oscillator strength for the trap level	f_{tr}	1
Width of the trap level (eV)	ν_{tr}	1.5
Nonlinear refractive index (cm^2/W)	n_2	3×10^{-16}

IV. RESULTS AND DISCUSSION

A. Test of the model

Figure 7 shows the relative phase shift and reflectivity of the S component of the probe beam for excitation intensities slightly lower (40 TW cm^{-2}) and moderately higher (57 TW cm^{-2}) than the damage threshold. Due to the coherent artifact discussed above, the data during the pump-probe time overlap have been kept away. The experimental data show a fast evolution during ≈400 fs after the excitation, followed by a steady regime on the picosecond scale. This corresponds to the fast promotion of electrons in the CB and relaxation toward some long-lived state (as shown in Fig. 6). Below the damage threshold, this state is similar to the initial one within the sensitivity of our diagnostic, but it is not the case above the threshold. The model described above contains the correct fast and slow timescales, but it clearly fails to describe the evolution at a level of excitation close to the damage threshold. During the fast response (the first 200 fs) corresponding to the electrons in the CB, the phase shift is correctly described at 40 TW cm^{-2} but underestimated at 57 TW cm^{-2}, and the reflectivity in the model is lower than unity in opposition with the experiment. During the steady phase, both the phase shift and the reflectivity are largely underestimated at 57 TW cm^{-2}.

We did not obtain a correct fitting of the data even when varying the main parameters of the model (maximum electron density in the CB, collision frequency, effective mass,

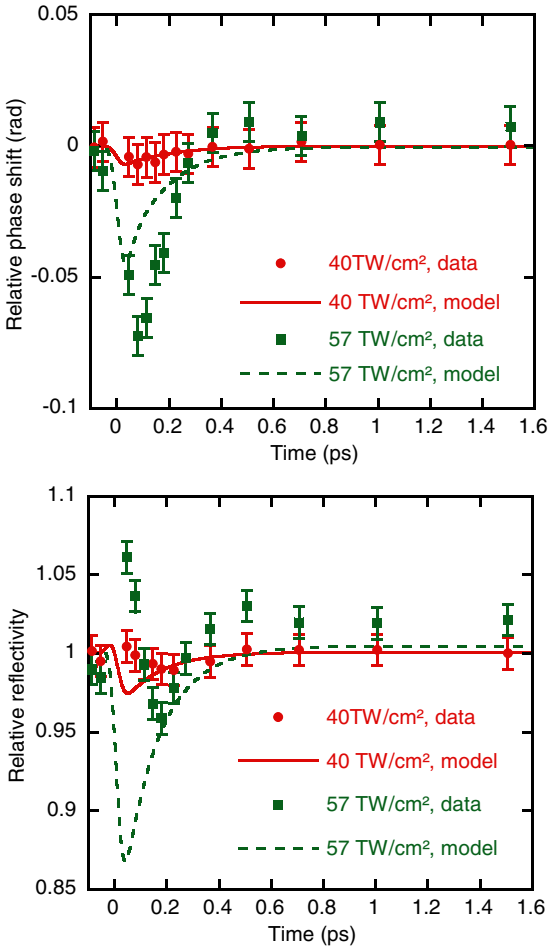

FIG. 7. Model assuming a frozen structure and a Drude-like response for the CB electrons, compared with experiment: Relative phase shift (top) and reflectivity (bottom) after excitation by 40 TW cm^{-2} (red dots and full line) and 57 TW cm^{-2} (green squares and dashed line) pump pulse. Only the S component of the probe is shown.

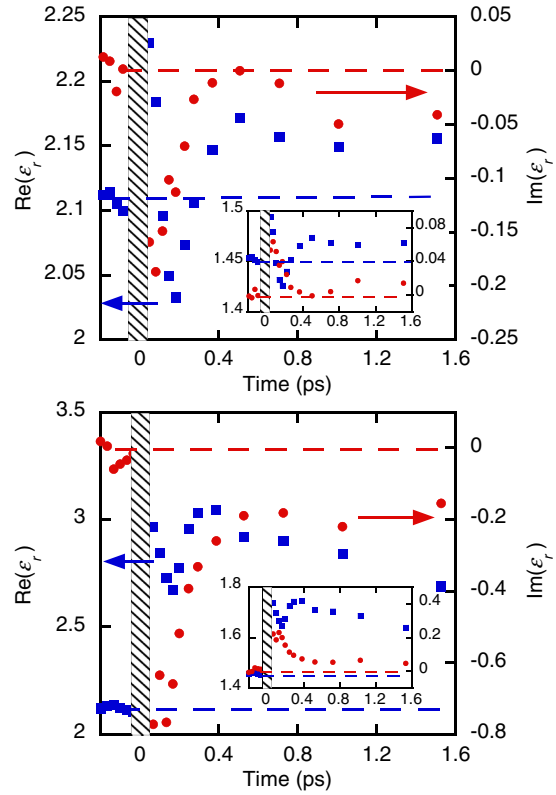

FIG. 8. Evolution of the dielectric function measured by the FDI experiment after excitation by 57 TW cm^{-2} (top) and 67 TW cm^{-2} (bottom). The corresponding optical indices are plotted in the insets. In each plot the imaginary part is showed by the red circles and refers to the left axis, whereas the real part corresponds to the blue squares and the right axis. The dashed lines show the values of the unexcited sample. The hatched rectangles correspond to the coherent artifact delays.

oscillator strength, and width of the trap level...). One most striking evidence for the misfit of the conceptual basis of the model is the increase in reflectivity during the first 200 fs after excitation: At such a short time, we can as a first approximation neglect the trapped states. This allows for reducing the number of remaining parameters in Eq. (2) and thus for evaluating them directly from the experimental data [see Eq. (A4) in Appendix A]. Within the model assumptions, this procedure gives unphysical (i.e., negative) values for the electron density in the CB. We stress that, unlike in the transmission interferometry, the reflected amplitude is here related mainly to the real part of the index: An increase in the reflectivity is associated with an increase in the real part of the index, in opposition with the contribution of the Drude term describing the electrons in the CB. This shows that whatever the parameters used in this model, its basement for the description of the dielectric function, which is the double-assumption of a frozen electronic structure and a Drude-like response for the CB electrons, is not valid in the high excitation regime.

B. Discussion

From our measurements, we are able to deduce the dielectric function ϵ_r at the sample surface without assumption [see Eq. (A1) in Appendix A]. The time evolution of the real and imaginary parts of the dielectric function at the probe wavelength (800 nm) is plotted in Fig. 8 for two intensities of the pump beam. The insets show the corresponding optical index $\sqrt{\epsilon_r}$. A complex scalar alone does not allow for disentangling the intricate mechanisms at play during the interaction between the optical wave and the excited material, however it could bring out some interesting—albeit somehow speculative—considerations about the dynamics of the excited sample after the excitation and the several possible reasons why the simple model described before fails to reproduce the results.

The imaginary part Im(ϵ_r) is related to the absorption of light (with our convention on the time dependence of the fields, a negative value corresponds to an absorbing medium). We see in the figure that, just after the excitation, the absorption is maximum then decreases in ≈400 fs. On the picosecond scale, it reaches a steady regime in which absorption increases with the initial excitation. This steady regime is reached in ≈400 fs after the 67-TW cm^{-2} excitation,

whereas it takes ≈1 ps to develop at 57 TW cm^{-2} after a low-absorption period around 500 fs. Since the probe beam intensity is not high enough to induce nonlinear interaction, the absorption is likely related to electrons in the CB or states in the gap close to the CB during the fast and quasisteady phases, respectively. The low-absorption period around 500 fs, visible at 57 TW cm^{-2}, suggests that the electrons are removed from the CB at a rate consistent with the ≈150-fs trapping time introduced in the previous model. Our data suggest also that the states in the gap related to the absorption during the quasisteady phase are created faster when the initial excitation is higher.

Turning now to the real part Re(ϵ_r), it is higher just after the excitation than the value for the unexcited sample. Then it decreases and re-increases during the ≈400-fs fast phase. After ≈500 fs, Re(ϵ_r) is nearly constant for the 57-TW cm^{-2} case and evolves quite slowly for the 67-TW cm^{-2} case. The transient minimum of Re(ϵ_r) during the fast phase increases with the intensity of the excitation. At 57 TW cm^{-2}, it is lower than the initial value, whereas it is higher after the 57-TW cm^{-2} excitation. In all cases, Re(ϵ_r) is always greater than zero, in opposition with the behavior of a metal or overdense plasma. This rather complex evolution of Re(ϵ_r) cannot be accounted for by the simple model described previously, and there are several possible causes. First, the interaction of the electrons in the CB and the probe light may be more complex than the Drude model lets us believe. The Drude formulation assumes a constant effective mass (which is related to the curvature of the band of the considered occupied state), which is generally not the case for states far from the lowest- or highest-energy levels of the CB. The effective mass can be negative if the band is locally concave, reversing the sign of the contribution of this state to the optical conductivity. Just after an intense excitation, a large number of electrons could be located far from the minimum of the CB. As a consequence, if the major contribution to ϵ_r is given by negative mass quasiparticles, we could expect its real part to increase, contrary to the usual plasma contribution. This could be a possible cause for the transient high value of Re(ϵ_r) just after the excitation. The following fast evolution of Re(ϵ_r) could be due to the relaxation of the electrons towards the low part of the CB (where their equivalent effective mass becomes gradually positive) and/or their trapping in localized states in the band gap, in the same way as after a low excitation. During their relaxation from high to lower states in the CB, the electrons could also cross some interband resonance, associated with an oscillating behavior of Re(ϵ_r). However this is not likely since it should be accompanied by a maximum of the absorption at the time of the inflection point (around 100 fs), which is not noticeable in our measurements. Second, theoretical predictions exist for several mechanisms of photoinduced electronic structure modification. For instance, *ab initio* electronic structure calculations of materials at finite electron temperatures predict a decrease in the band gap of more than 1.5 eV in diamond for an electron temperature of 3 eV [23]. This calculation is based on the GW approximation [36], and the method is known to generate very accurate band structures of material at zero temperature. We stress that, in the finite electron temperature calculation, the atomic positions are fixed, and the gap decrease is uniquely due to the presence of electrons in the CB through the variation in the exchange self-energy and the increase in screening, independent of any phase transition. A gap shrinking produces an increase in Re(ϵ_r), and since the process is expected to be quasi-instantaneous, it could explain the fast response that we observed. Note that the temperature dependence of the optical index of fused silica [37] shows that a vibrational activation associated with the excitation of the material could also increase Re(ϵ_r). However, after a femtosecond excitation we expect the vibrational activity to increase monotonically with time as the energy flows from the electrons to the lattice and thus Re(ϵ_r). This is obviously not what we observe, thus this contribution should be of minor importance compared to those evoked just before.

Finally, the slower response (picosecond scale) may be attributed to the defect formation. Indeed this component is nonzero only above 45 TW cm^{-2}, the threshold for permanent damage. The formation of defects within a picosecond after an electron excitation has been observed in *ab initio* molecular dynamics (MD) simulation in vitreous silica [8]. The authors show an increase in the real and imaginary parts of the optical index as we observed on the picosecond timescale. The defects were identified as Si E' centers and nonbridging oxygen hole centers, which introduce a large number of discrete levels within the band gap of silica glass and induce a multicomponent absorption spectrum. In the MD simulation, the electron temperature was maintained at $T_{el} = 25\,000$ K during 300 fs then quenched at 300 K. The time of excitation was long enough to initiate the movement of the atoms, which leads to the defects after a time, even if the electron excitation is not maintained. Thus the fast decay of electrons from the CB as suggested by the decrease in Im(ϵ_r) does not prevent the defects' formation. Actually, the decay towards STE could help the defect formation by localizing the excitation energy [38].

V. SUMMARY AND CONCLUSION

To summarize, we performed femtosecond pump-probe interferometry in a reflection geometry on fused-silica samples. We focus our paper on the regime just below the damage threshold as well as between the damage and the ablation thresholds. The threshold values are ensured by postmortem analysis as well as comparison of the FDI measurements in two directions of polarizations. After a blackout due to diffraction onto a transient grating during the time overlap between the pump and the probe pulses, the simultaneous measurement of both the phase and the amplitude allows the determination of the evolution after the excitation of the real and imaginary parts of the dielectric function at the probe wavelength (800 nm). Our experimental data strongly constrain the modeling of electron dynamics in the sample and demonstrate the failure in the interaction regime, studied in this paper, of the widely used modeling for the dielectric function based on a fixed electronic band structure and a Drude-like behavior of the electron in the conduction band. The measurement of the dielectric function only is not enough to disentangle the complexity of the mechanisms at play beyond the simple model. However our measurements suggest that the fast response could be due to excited electrons far from the minimum of the conduction band and/or a band-gap

shrinking caused by the electron population in the CB. The slower response (i.e., on the picosecond scale) could be due to a band-gap filling associated with the defects' formation in the material.

ACKNOWLEDGMENTS

We acknowledge R. Bouillaud, F. Burgy, and L. Merzeau for their technical assistance and J. Gaudin for lending us a Nomarsky microscope. This work was supported by the French Agence Nationale de la Recherche under Grant OEDYP (Grant No. ANR-09-BLAN-0206-01) as well as the Conseil Régional d'Aquitaine, under Grants POLUX (Grant No. 2010-13-04-002) and COLA2 (Grant No. 2.1.3 09010502).

APPENDIX A: DATA REDUCTION

Our diagnostic measures four quantities: amplitude and phase shift in two polarizations. The comparison of both polarizations allows for validating the use of the Fresnel relations. In this case, we can deduce the experimental dielectric function ϵ_{FDI} by inverting the Fresnel relations [28],

$$\epsilon_{\mathrm{FDI}} = \Omega_S/\Omega_P, \tag{A1}$$

where $\Omega_{S,P} = (1 - R^*_{S,P})/(1 + R^*_{S,P})$ with $R^*_{S,P} = R_{S,P}e^{i\phi^{\mathrm{opt}}_{S,P}}$. $\phi^{\mathrm{opt}}_{S,P}$ is given by Eq. (2).

In the framework of the model tested in Sec. IV A at the short delays when the trapped states can be neglected, Eq. (2) reduces to

$$\epsilon^F_{\mathrm{FDI}} = \epsilon_{r0} - \tilde{n_e}/(1 - i\tilde{\nu}), \tag{A2}$$

where $\tilde{\nu} = \nu_{\mathrm{CB}}/\omega$ and $\tilde{n_e} = n_{\mathrm{CB}}/n_c$ with n_c as an effective critical electron density $n_c = \epsilon_0 m^*\omega^2/e^2 f_{\mathrm{CB}} = m^*/m f_{\mathrm{CB}} \times n_{\mathrm{ipc}}$. We can rearrange Eq. (A2) to get

$$\begin{aligned} \tilde{\nu} &= -\mathrm{Im}\left(\epsilon^F_{\mathrm{FDI}}\right)/\left[\epsilon_{r0} - \mathrm{Re}\left(\epsilon^F_{\mathrm{FDI}}\right)\right], \\ \tilde{n_e} &= -\mathrm{Im}\left(\epsilon^F_{\mathrm{FDI}}\right)(1 + \tilde{\nu}^2)/\tilde{\nu}, \end{aligned} \tag{A3}$$

where $\mathrm{Re}(\epsilon^F_{\mathrm{FDI}})$ and $\mathrm{Im}(\epsilon^F_{\mathrm{FDI}})$ are the real and imaginary parts of $\epsilon^F_{\mathrm{FDI}}$. If we assume that the electronic structure is the same as in the unexcited material (frozen structure assumption) and that the density in the CB is very small compared to the density in the VB, we set ϵ_{r0} to the value of the dielectric function in the unexcited sample $\epsilon_{r0} = 2.11$ and deduce $\tilde{\nu}$ and $\tilde{n_e}$.

APPENDIX B: INDUCED GRATING

Let us consider the pump beam (intensity I_p, angle of incidence θ_p, and wavelength λ) striking the target surface synchronously with the probe pulse (angle of incidence θ_s, wavelength λ, intensities I^S_s and I^P_s, respectively, in the S and P probe components of polarization). In our experiment, $I^P_s \approx I^S_s \equiv b^2 I_p$ with $b \approx 0.1$. The pump and probe pulses add coherently at the target surface to yield the intensity $I(x) = I_p[1 + 2b\cos(2\pi x/d)]$ at the first order in b, where x is the spatial coordinate along the target surface and the plane of incidence of the beams and the fringe distance d,

$$1/d = |\sin\theta_s - \sin\theta_p|/\lambda. \tag{B1}$$

This excitation induces optical properties modifications which we describe by the local complex optical index,

$$N[I(x)] = N(I_p) + \frac{dN}{dI}(I_p)2bI_p\cos\left(\frac{2\pi x}{d}\right), \tag{B2}$$

and the corresponding local complex reflectivity,

$$r^{S,P}_\theta[I(x)] = r^{S,P}_\theta(I_p) + \delta r^{S,P}_\theta\cos\left(\frac{2\pi x}{d}\right) \tag{B3}$$

[note that $r^{S,P}_\theta(I_p)$ and $\delta r^{S,P}_\theta$ depend on the angle of incidence θ of the reflected beam as well as its polarization S or P]. Due to this modulated reflectivity the target surface behaves like a grating whose response in the zero order is proportional to $r(I_p)$ and $\delta r/2$ in the first order of diffraction. As the grating is generated by the overlap of the pump and probe beams, the grating equation is automatically fulfilled for these beams: For an incident probe beam, the order one of diffraction is in the direction of the pump beam and reciprocally. Finally, noting that due to the incidence angles of the beams in our setup, there is no light reflected in the second orders, the amplitude collected by the detector in the output direction of the probe beam is as follows:

$$E^{S,P}_c \approx \left[r^{S,P}_{45}(I_p) - \frac{\delta r^{S,P}_{45}}{2}\right]E^{S,P}_s + \frac{\delta r^{S,P}_5}{2}E^{S,P}_p, \tag{B4}$$

where the superscripts denote the direction of polarization and the subscripts in the fields are for the beam (c for collected, s for the incident probe, and p for the incident pump). The first term on the right side of Eq. (B4) stands for the reflected probe beam, the second term is the probe light lost by refraction, and the third is the refracted pump light. Since the typical variation of the relative reflectivity shown in Fig. 4 (top) is a few percentages, we assume that the local reflectivity Eq. (B3) is close to the initial reflectivity of the unexcited surface $r^{S,P}_{0,\theta}$ and omitting for clarity the indices for θ and the polarization, we write

$$r(x) = r_0 + \frac{dr}{dN}(N_0)\{N[I(x)] - N_0\}, \tag{B5}$$

with N_0 as the optical index of the unexcited surface. Using Eq. (B2) we get

$$\begin{aligned} r(x) = r_0 &+ \frac{dr}{dN}(N_0) \\ &\times\left[N(I_p) - N_0 + \frac{dN}{dI}(I_p)2bI_p\cos\left(\frac{2\pi x}{d}\right)\right], \end{aligned} \tag{B6}$$

and by identification with Eq. (B3),

$$r(I_p) = r_0 + \frac{dr}{dN}(N_0)[N(I_p) - N_0], \tag{B7}$$

$$\delta r = \frac{dr}{dN}(N_0)\frac{dN}{dI}(I_p)2bI_p. \tag{B8}$$

To describe the nonlinear response of the material, we use the Taylor expansion of $N(I)$,

$$N(I) = N_0 + \sum_{k>0} N_{2k}I^k, \tag{B9}$$

and we assume that we can keep only the dominant k term $N(I) \approx N_0 + N_{2k}I^k$. Above the damage threshold, we expect a high level of electron excitation which is responsible for the value of $N(I)$ and k should be greater than (or equal to) the ratio of the gap energy over the photon energy (six for a SiO_2

sample irradiated by an 800-nm laser). Then $\frac{dN}{dI}(I_p)2bI_p = 2bk[N(I_p) - N_0]$ in Eq. (B8), and the amplitude collected by the detector writes

$$E_c^{S,P} \approx \left\{ r_{45}^{S,P}(0) + \frac{dr_{45}^{S,P}}{dN}(N_0)[N(I_p) - N_0](1 - bk) \right\} \times E_s^{S,P} + \frac{dr_5^{S,P}}{dN}(N_0) N_{2k} I_p^k k b E_p^{S,P}. \quad \text{(B10)}$$

The reflectivity measured with our apparatus is defined as $r_{\mathrm{FDI}}^{S,P} = \frac{1}{r_{45}^{S,P}(0)} \frac{E_c^{S,P}}{E_s^{S,P}}$. For sufficiently high-order k, bk is on the order of unity and since $E_p^P = 0$ and $E_p^S = E_s^S/b$, it follows from Eq. (B10) that the responses in P and S are largely underestimated and overestimated, respectively, during the pump and probe overlap as we observed in our experiment.

[1] L. V. Keldysh, Sov. Phys. JETP **20**, 1307 (1965).
[2] P. Audebert, P. Daguzan, A. Dos Santos, J. C. Gauthier, J. P. Geindre, S. Guizard, G. Hamoniaux, K. Krastev, P. Martin, G. Petite, and A. Antonetti, Phys. Rev. Lett. **73**, 1990 (1994).
[3] B. C. Stuart, M. D. Feit, S. Herman, A. M. Rubenchik, B. W. Shore, and M. D. Perry, Phys. Rev. B **53**, 1749 (1996).
[4] P. Martin, S. Guizard, P. Daguzan, G. Petite, P. D'Oliveira, P. Meynadier, and M. Perdrix, Phys. Rev. B **55**, 5799 (1997).
[5] M. Lenzner, J. Kruger, S. Sartania, Z. Cheng, C. Spielmann, G. Mourou, W. Kautek, and F. Krausz, Phys. Rev. Lett. **80**, 4076 (1998).
[6] A. Kaiser, B. Rethfeld, M. Vicanek, and G. Simon, Phys. Rev. B **61**, 11437 (2000).
[7] R. Stoian, A. Rosenfeld, D. Ashkenasi, I. V. Hertel, N. M. Bulgakova, and E. E. B. Campbell, Phys. Rev. Lett. **88**, 097603 (2002).
[8] S. Sen and J. E. Dickinson, Phys. Rev. B **68**, 214204 (2003).
[9] A. Q. Wu, I. H. Chowdhury, and X. Xu, Phys. Rev. B **72**, 085128 (2005).
[10] V. V. Temnov, K. Sokolowski-Tinten, P. Zhou, A. El-Khamhawy, and D. von der Linde, Phys. Rev. Lett. **97**, 237403 (2006).
[11] M. Boero, A. Oshiyama, P. L. Silvestrelli, and K. Murakami, Physica B (Amsterdam) **376**, 945 (2006).
[12] B. Rethfeld, Phys. Rev. B **73**, 035101 (2006).
[13] G. M. Petrov and J. Davis, J. Phys. B: At., Mol. Opt. Phys. **41**, 025601 (2008).
[14] L. Jiang and H.-L. Tsai, J. Appl. Phys. **104**, 093101 (2008).
[15] D. Grojo, M. Gertsvolf, S. Lei, T. Barillot, D. M. Rayner, and P. B. Corkum, Phys. Rev. B **81**, 212301 (2010).
[16] B. Chimier, O. Utéza, N. Sanner, M. Sentis, T. Itina, P. Lassonde, F. Légaré, F. Vidal, and J. C. Kieffer, Phys. Rev. B **84**, 094104 (2011).
[17] B. Rethfeld, A. Rämer, N. Brouwer, N. Medvedev, and O. Osmani, Nucl. Instrum. Methods Phys. Res., Sect. B **327**, 78 (2014).
[18] A. Sommer, E. M. Bothschafter, S. A. Sato, C. Jakubeit, T. Latka, O. Razskazovskaya, H. Fattahi, M. Jobst, W. Schweinberger, V. Shirvanyan, V. S. Yakovlev, R. Kienberger, K. Yabana, N. Karpowicz, M. Schultze, and F. Krausz, Nature (London) **534**, 86 (2016).
[19] M. Lucchini, S. A. Sato, A. Ludwig, J. Herrmann, M. Volkov, L. Kasmi, Y. Shinohara, K. Yabana, L. Gallmann, and U. Keller, Science **353**, 916 (2016).
[20] M. Garcia-Lechuga, L. Haahr-Lillevang, J. Siegel, P. Balling, S. Guizard, and J. Solis, Phys. Rev. B **95**, 214114 (2017).
[21] T. Winkler, L. Haahr-Lillevang, C. Sarpe, B. Zielinski, N. Götte, A. Senftleben, P. Balling, and T. Baumert, Nat. Phys. **14**, 74 (2018).
[22] A. Bourgeade and G. Duchateau, Phys. Rev. E **85**, 056403 (2012).
[23] S. V. Faleev, M. van Schilfgaarde, T. Kotani, F. Léonard, and M. P. Desjarlais, Phys. Rev. B **74**, 033101 (2006).
[24] E. N. Glezer, Y. Siegal, L. Huang, and E. Mazur, Phys. Rev. B **51**, 6959 (1995).
[25] J. P. Geindre, P. Audebert, A. Rousse, F. Falliès, J. C. Gauthier, A. Mysyrowicz, A. D. Santos, G. Hamoniaux, and A. Antonetti, Opt. Lett. **19**, 1997 (1994).
[26] F. Deneuville, B. Chimier, D. Descamps, F. Dorchies, S. Hulin, S. Petit, O. Peyrusse, J. J. Santos, and C. Fourment, Appl. Phys. Lett. **102**, 194104 (2013).
[27] C. Fourment, F. Deneuville, D. Descamps, F. Dorchies, S. Petit, O. Peyrusse, B. Holst, and V. Recoules, Phys. Rev. B **89**, 161110(R) (2014).
[28] C. Fourment, F. Deneuville, B. Chimier, D. Descamps, F. Dorchies, S. Hulin, S. Petit, O. Peyrusse, and J. J. Santos, Proc. SPIE **8777**, 87770M (2013).
[29] Z. Vardeny and J. Tauc, Opt. Commun. **39**, 396 (1981).
[30] H. Eichler, D. Langhans, and F. Massmann, Opt. Commun. **50**, 117 (1984).
[31] S. V. Govorkov, I. L. Shumai, W. Rudolph, and T. Schroder, JETP Lett. **52**, 117 (1990).
[32] I. H. Malitson, J. Opt. Soc. Am. **55**, 1205 (1965).
[33] L. Barilleau, G. Duchateau, B. Chimier, G. Geoffroy, and V. Tikhonchuk, J. Phys. D: Appl. Phys. **49**, 485103 (2016).
[34] L. A. A. Pettersson, L. S. Roman, and O. Inganäs, J. Appl. Phys. **86**, 487 (1999).
[35] D. Milam, Appl. Opt. **37**, 546 (1998).
[36] L. Hedin, Phys. Rev. **139**, A796 (1965).
[37] B. Sadigh, P. Erhart, D. Åberg, A. Trave, E. Schwegler, and J. Bude, Phys. Rev. Lett. **106**, 027401 (2011).
[38] S. Mao, F. Quéré, S. Guizard, X. Mao, R. Russo, G. Petite, and P. Martin, Appl. Phys. A **79**, 1695 (2004).